The 8th European Congress on Computational Methods in Applied Sciences and Engineering
ECCOMAS Congress 2022
5-–9 June 2022, Oslo, Norway

EFFECTS OF UNCERTAINTIES OF IMAGE-BASED MATERIAL PROPERTIES OF GREAT VESSELS ON VASCULAR DEFORMATION

B.M. Fanni[1], M.N. Antonuccio[1], G. Santoro[2], A. Mariotti[3], M.V. Salvetti[3] and S.Celi[1]

[1] BioCardioLab - Bioengineering Unit, Ospedale del Cuore, Fondazione CNR - Regione Toscana G. Monasterio, Via Aurelia Sud, 54100 Massa, Italy
bmfanni@ftgm.it, mnantonuccio@ftgm.it, s.celi@ftgm.it

[2] Pediatric Cardiology Unit, Ospedale del Cuore, Fondazione CNR - Regione Toscana G. Monasterio, Via Aurelia Sud, 54100 Massa, Italy, gsantoro@ftgm.it

[3] Department of Civil and Industrial Engineering, University of Pisa, Via G. Caruso 8, 56122, Pisa, Italy, alessandro.mariotti@unipi.it, maria.vittoria.salvetti@unipi.it

Key words: imaging, material properties, UQ, FSI, cardiovascular, aorta

Abstract. Patient-specific computational models represent a powerful tool for the planning of cardiovascular interventions. In this context, the patient-specific material properties are considered as one of the biggest source of uncertainty.
In this work, we investigated the effect of the uncertainty of the elastic module (E), as computed from a recent image-based methodology, on a fluid-structure interaction (FSI) model of a patient-specific aorta. The Uncertainty Quantification (UQ) was carried out using the generalized Polynomial Chaos (gPC) method. Four deterministic simulations were run based on the four quadrature points, computed considering a deviation of $\pm 20\%$ on the estimation of the E value of the vessel wall from patient's imaging.
The UQ of the E parameter was evaluated on the area and flow variations among cardiac cycle extracted from five cross-sections of the aortic FSI model. Results from gPC analysis showed a not significant variation of the area and flow quantities during the whole cardiac period, thus demonstrating the effectiveness of the used image-based methodology in the inferring of the E parameter, despite its intrinsic errors due to model definition.
This study highlights the importance of imaging to retrieve useful data in an indirect and non-invasive way, to enhance the reliability of in-silico models in the clinical practice.

1 INTRODUCTION

Over the last years, patient-specific computational models have kept spreading, potentially representing a powerful tool for a wide range of cardiovascular applications [1, 2, 3, 4, 5]. The recent advances of medical imaging and numerical power have allowed the spread of numerical patient-specific modeling, thus providing a reliable tool for the study of cardiovascular problems in a highly accurate way.

Among the large number of information required to implement the numerical model, patient-specific material properties of implantation site still represent the major challenge [6, 7, 8]. In fact, while the current imaging techniques allow a high-fidelity depiction of the in-vivo anatomy of the patient, a proper patient-specific numerical replica requires also a reliable implementation of boundary conditions and material properties, with this latter at date representing the biggest source of uncertainty [9, 10].

Recently, a novel image-based tool was developed to infer directly and non-invasively the mechanical properties of vessel wall [11], representing a valuable strategy to determine the proper patient-specific material properties in an in-silico model. However, such methodology still presents a gap between the estimated material model and the ground of truth, due to the intrinsic modeling features and image-related uncertainties. In this work, we investigated the effect of such uncertainties using uncertainty quantification (UQ) techniques, to evaluate the reliability of the method.

2 THEORETICAL BACKGROUND

2.1 The χ-Method

The χ-method is a recent image-based technique able to infer in a non-invasive and direct way the local elastic properties (in terms of elastic module E) of vascular walls. The methodology was the results of the previous studies available at [12, 11], based on the exploitation and refinement of the so-called QA method.

The QA method was firstly presented as a technique able to estimate the pulse wave velocity (PWV) from phase contrast magnetic resonance imaging (PC MRI) [13] and ultrasound images [14]. According to the QA method, the relationship during the reflection-free early systole period of the cardiac cycle between the cross-sectional area A of the vessel and the passing flow Q can be approximated as a first-order linear equation. Hence, the PWV can be computed as:

$$PWV = \left.\frac{dQ}{dA}\right|_{\text{early systole}} \tag{1}$$

where dA is the incremental variation of the cross-sectional area and dQ is the incremental variation of the flow passing through the section.

According to literature [**?**], an estimation of the E value of the vessel can be estimated as function of PWV and some features of the vessel:

$$E_{PWV} = 3\,\rho\,PWV^2\left(1 + \frac{A_0}{WCSA}\right) \tag{2}$$

in which ρ is the density of the fluid passing through the cross-section of the vessel, A_0 is the area of vessel's lumen and $WCSA$ is the wall cross-sectional area (i.e. the area between inner and outer diameter), both measured at diastole.

Following the preliminary results available in the previous studies [12, 11], a correction factor was included in the Equation 2 to make the formula more predictive of the E value of the vessel wall, defined as:

$$\chi = \gamma\,RAC \tag{3}$$

where RAC is the relative area change along the cardiac cycle and γ is a function of some model characteristics such as geometry, flow and pressure quantities.
Hence, the enhanced formula for the estimation of the E value is provided multiplying the Equations 2 and 3:

$$E_\chi = 3\,\gamma\,RAC\,\rho\,PWV^2\left(1+\frac{A_0}{WCSA}\right) \tag{4}$$

The χ-method is able to estimate the local E value of a vessel wall at a selected cross-section, using the Equation 1, which considers the PWV as computed from the QA method, specific geometrical features of the section, and a crucial corrective factor χ.

2.2 Generalized Polynomial Chaos Expansion

To investigate the impact of image-related uncertainties on the outcomes of the χ-method, the generalized Polynomial Chaos Expansion (gPC) was used, consisting in a generation of stochastic response surface. The evaluation of the continuous surface response consists in three steps: (i) calculation of the quadrature points; (ii) deterministic simulations; (iii) assessment of the gPC for the quantity of interest X, expressed as:

$$X(\omega) = \sum_{r=0}^{\infty} a_r \mathbf{\Phi}_r(\zeta(\omega)) \tag{5}$$

where ω is an elementary event, $\zeta(\omega)$ is an unbounded random vector of uncertain parameters, $\mathbf{\Phi}_r$ is the r-th orthogonal polynomial basis and a_r is the related coefficient. Given the orthogonality property of the polynomial basis, the coefficient a_r can be computed as:

$$a_r = \frac{\langle X, \mathbf{\Phi}_r\rangle}{\langle \mathbf{\Phi}_r, \mathbf{\Phi}_r\rangle} = \frac{1}{\langle \mathbf{\Phi}_r, \mathbf{\Phi}_r\rangle}\int_{\mathrm{supp}(\zeta)} \mathbf{\Phi}_k(\zeta)\eta(\zeta)\delta(\zeta) \tag{6}$$

where $supp(\zeta)$ is the integration domain, i.e. the support of the random vector ζ and $\eta(\zeta)$ is the weight function ensuring the orthogonality for the specific polynomial function.

The Probability Distribution Function (PDF) of the studied uncertain parameters was assumed as uniform due to the unavailability of statistical information, and the uniform PDF is the least informative distribution able to provide the highest variance in given intervals. Consequently, the Legendre polynomials were used as polynomial basis, truncating to the third order for each dimension. Hence, four quadrature points were used for the uncertain variable.

3 MATERIAL AND METHODS

The investigated scenario was comprehensive of all the uncertain variables somehow affecting the outcomes of the χ-method in terms of reliability of the computed E value. In fact, as observed in the results of the previous work [11], a deviation from the ground of truth is still present. Hence, although a relative error not greater than 15% was found for the difference from the ground of truth, for this UQ study a standard deviation of 20% was assumed in the calculation of the E_χ value (Equation 4).

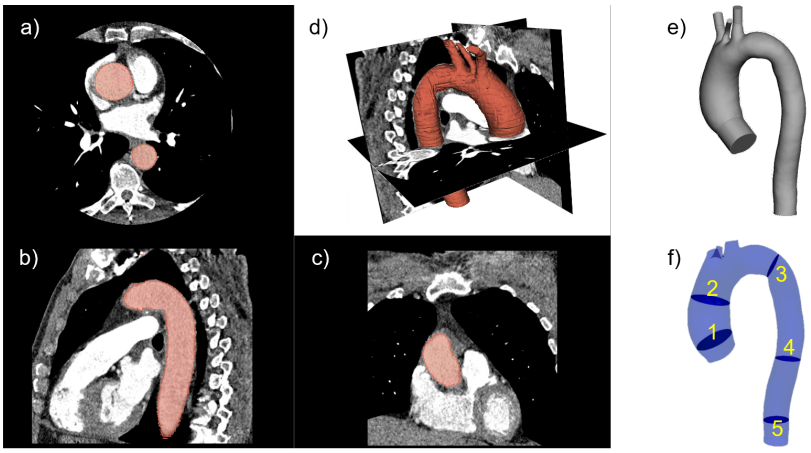

Figure 1: CT images at anatomical planes **(a-b-c)** and resulted raw segmentation of the aorta **(d)**, refined model for simulation **(e)** and indication of the analyzed slices **(f)**.

A patient-specific case was analyzed, consisting in a computed tomography dataset for the geometry modeling of the aorta (Figure 1) and PC MRI data at aortic valve for the estimation of the E_χ value and boundary conditions of the computational model (Figure 2).

The evaluation of the phase contrast data led to an estimation of the E_χ value of 2.02 MPa, according to the χ-method [11]. An isotropic linear elastic material was adopted for the 2 mm thickness wall, with a Poisson's ratio of 0.49. Four different E values were assigned, corresponding to the quadrature points computed considering the range [$E_\chi-$ 20%; $E_\chi+$ 20%], as listed in Table 1.

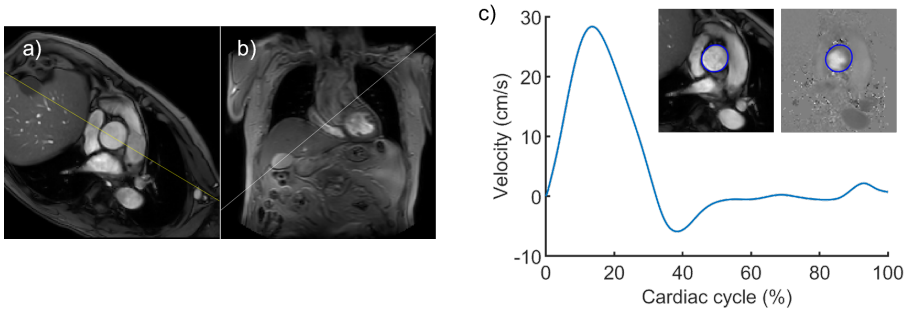

Figure 2: Extraction of the plane acquisition **(a)** from the localizer sequence **(b)** and velocity curve at aortic valve extracted from the segmentation of phase contrast MRI data **(c)**.

The blood was considered incompressible and non Newtonian (ρ = 1060 kg m^3 and μ = 0.05 kg m^{-1} s^{-1}) [15, 16]. The fluid mesh (ANSA, Beta CAE Systems) consisted in 3,524,413 tetrahedral elements, with dimensions ranging from 1.0 to 1.5 mm, based on model curvature. Five inflation layers were set to model boundaries. A node-to-node correspondence between structural and fluid domain was assured.

Table 1: Quadrature points related to the E values assigned to the vessel wall of the deterministic FSI simulations.

	Quadrature points			
E (MPa)	1.61	1.86	2.17	2.42

No degrees of freedom were allowed to the edges of the structural mesh. The boundary conditions of the CFD model were set according to the MRI-based velocity at the inlet and four different Windkessel models at the outlets. The RCR values were opportunely tuned to get a physiological pressure range and waveform at each outlet (Table 2).

Table 2: RCR values of the Windkessel models for the boundary conditions assigned to the aorta outlets: the three supra-aortic vessels, i.e. the brachiocephalic artery, the left common carotid artery and the left subclavian artery and the descending aorta.

	R_p (Kg s^{-1} m^{-4})	C (m^3 Pa $^{-1}$)	R_d (Kg s^{-1} m^{-4})
Brachiocephalic artery	$1.3 \cdot 10^7$	$1.5 \cdot 10^{-9}$	$1.3 \cdot 10^9$
Left common carotid artery	$5.1 \cdot 10^7$	$3.8 \cdot 10^{-10}$	$5.0 \cdot 10^9$
Left subclavian artery	$1.1 \cdot 10^7$	$1.7 \cdot 10^{-9}$	$1.1 \cdot 10^9$
Descending aorta	$2.5 \cdot 10^6$	$7.7 \cdot 10^{-9}$	$2.4 \cdot 10^8$

Each simulation corresponding to one quadrature point was run for 10 cardiac cycles to make the RCR models reaching the regime state. A time step of 0.5 ms was set for both fluid and mechanical solvers. The response surfaces were calculated for area and flow-rate variations via Dakota, at specific five different numbered slices extracted along the centerline of the model.

4 RESULTS AND DISCUSSION

The UQ results are reported in terms of PDF and standard deviation at each time instant of the cardiac cycle for area and flow variations. PDF values represent the non-normalized probability that the output of the model expresses a specific value, due to the uncertainty effect.

The UQ analysis was based on the unknown variables affecting the prediction of the χ-method for the inferring of the E value from imaging data.

The flow-rate was minimally affected by the uncertainties related to the stiffness wall estimation. A modest variance was encountered for slice 2, as reported in Figures 4, reasonably due to the complex flow arising from the enlargement of ascending aorta (the patient was affected by a mild aneurysm), making the local velocity patterns slightly dependent on the vessel compliance. On the contrary, none fluctuation was found for the rest of the slices, presenting a regular flow, whose PDFs and standard deviations are showed in Figures 3c-d, 5c-d, 6c-d and 7c-d for slice 1, 3, 4 and 5, respectively.

A moderate area variation resulted from the effect of the E-related uncertainties. This effect appeared to be more pronounced for the larger slices, with slice 2 presenting the most spread PDF and standard deviation (Figures 4a-b), following by slice 1 (Figures 3a-b). However, the overall influence of the uncertainties due to $\chi-$method on the area deformation was found to

be relatively restrained and almost totally negligible for the slices selected after the aortic arch, characterized by a regular lumen and a straight vessel centerline (Figures 5a-b, 6a-b and 7a-b).

Notwithstanding, the need of reducing, at least partially, the level of uncertainties is still required, especially the effect of the unknown thickness wall, which is predominant in the variance introduced in the area deformation.

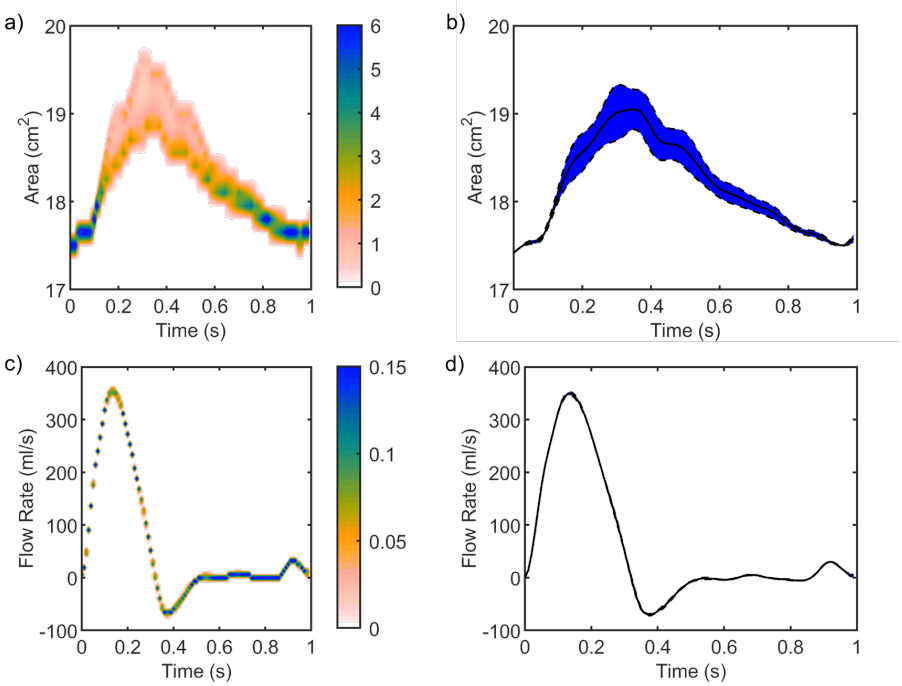

Figure 3: PDFs (left panels) and standard deviations (right panels) at each time instant of the cardiac cycle for area **(a-b** and flow **(c-d)** variations, as extracted from slice 1.

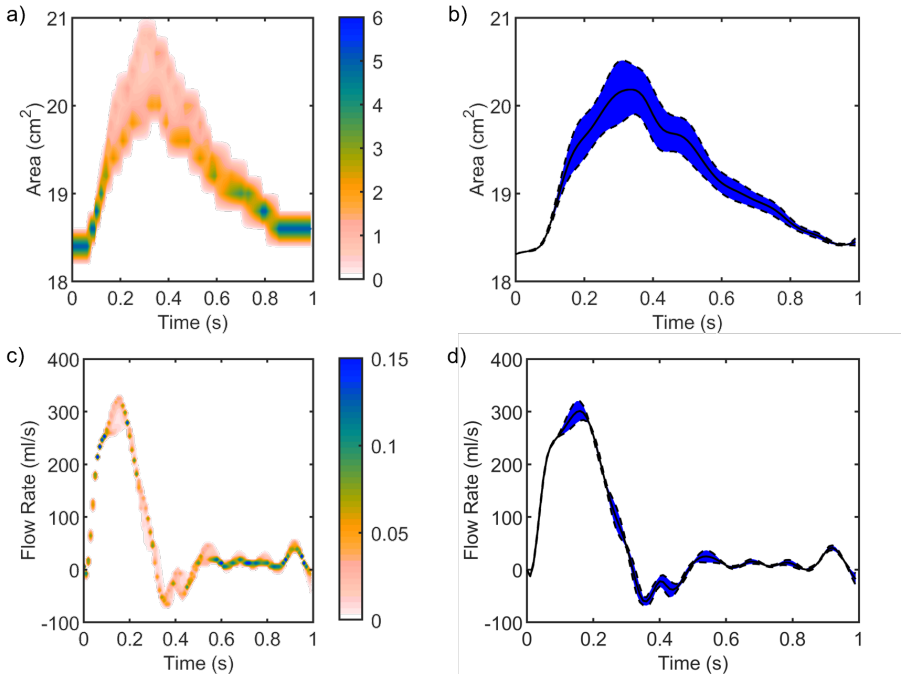

Figure 4: PDFs (left panels) and standard deviations (right panels) at each time instant of the cardiac cycle for area **(a-b** and flow **(c-d)** variations, as extracted from slice 2.

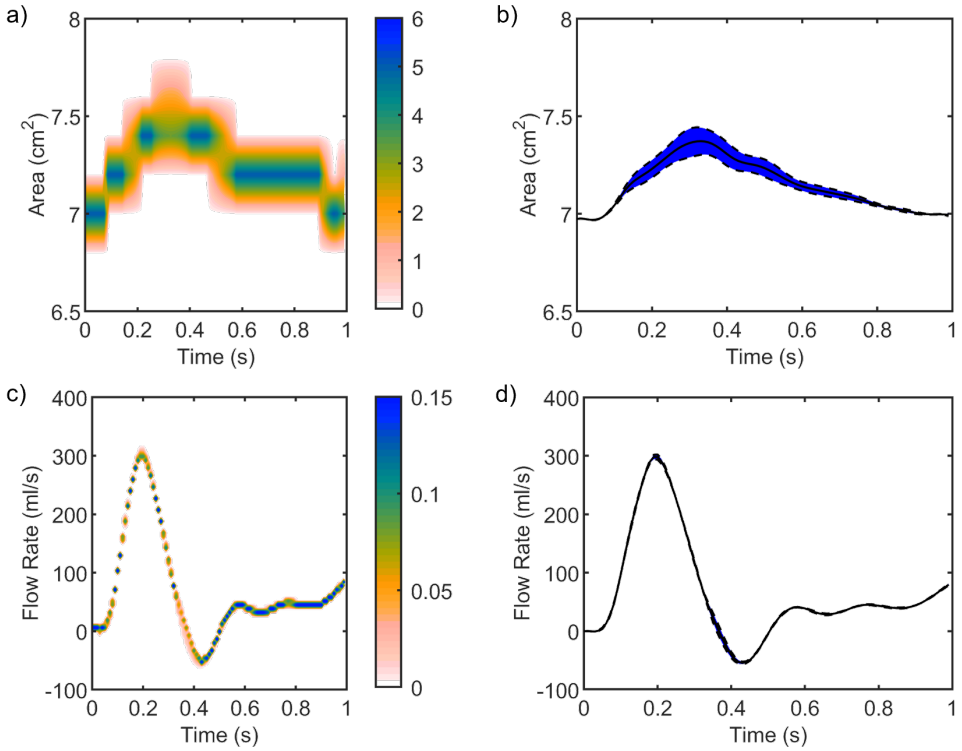

Figure 5: PDFs (left panels) and standard deviations (right panels) at each time instant of the cardiac cycle for area **(a-b** and flow **(c-d)** variations, as extracted from slice 3.

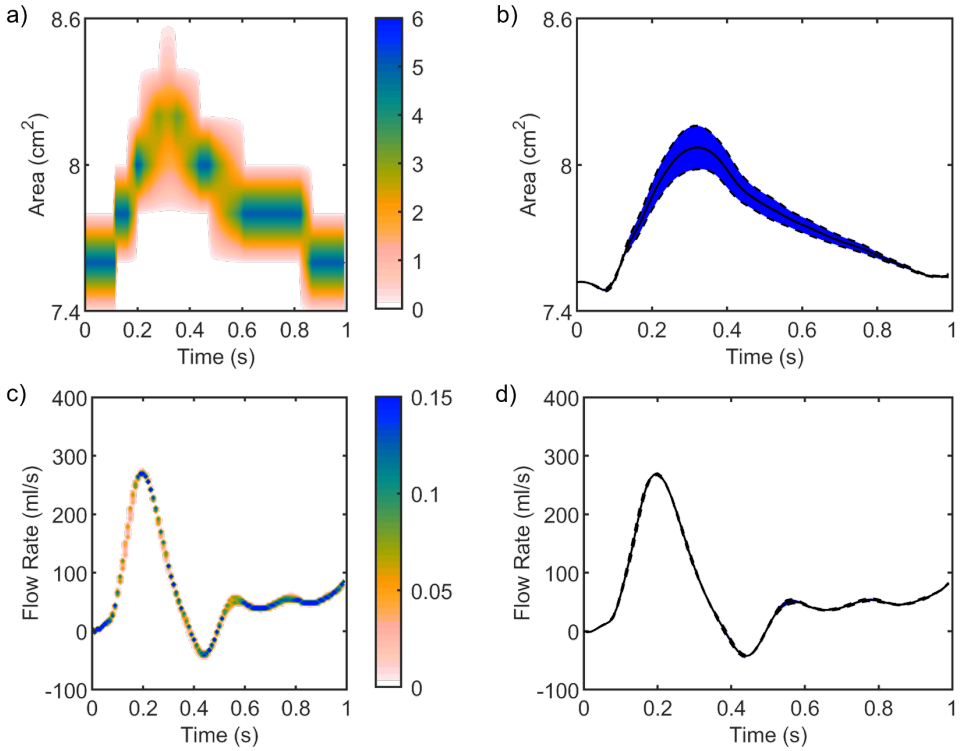

Figure 6: PDFs (left panels) and standard deviations (right panels) at each time instant of the cardiac cycle for area **(a-b** and flow **(c-d)** variations, as extracted from slice 4.

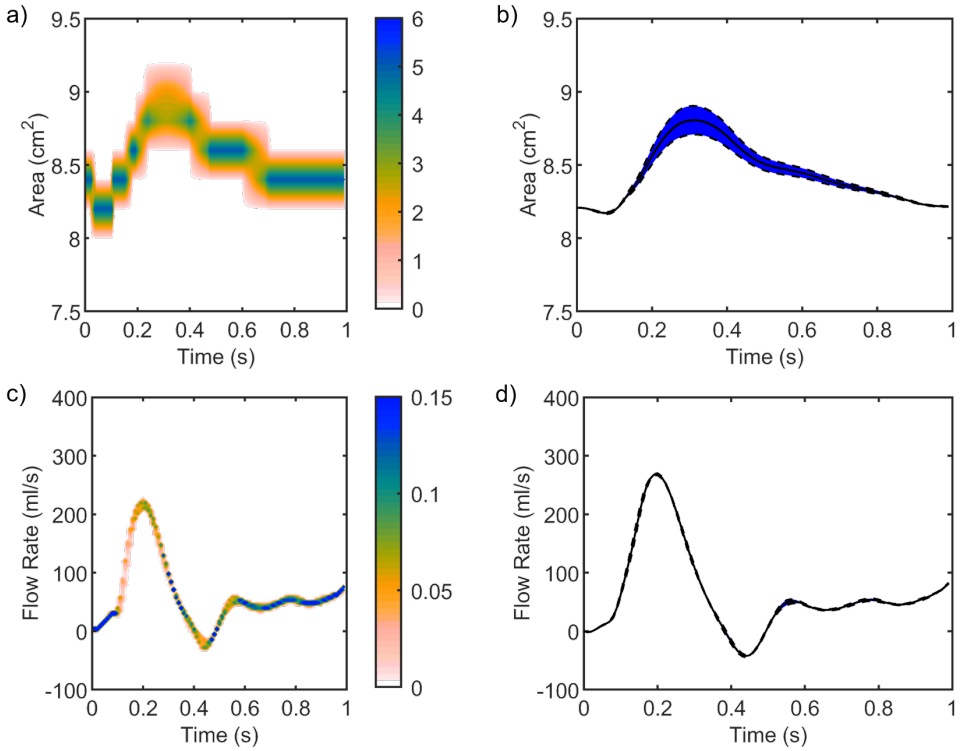

Figure 7: PDFs (left panels) and standard deviations (right panels) at each time instant of the cardiac cycle for area **(a-b** and flow **(c-d)** variations, as extracted from slice 5.

5 CONCLUSIONS

In this work we used gPC to evaluate the effect of image-related uncertainty of the χ-method on the area deformation and flow variations of a patient-specific aortic model. Results showed that, while the flow-rate was barely affected by the input uncertainties, area deformation was subjected to a non-negligible effect, especially at ascending aorta. However, such deviation can be considered relatively restrained, although further investigation to reduce such undesired effects will be conducted.

UQ techniques represent a valuable strategy to investigate the level of reliability of numerical patient-specific models, thus pointing out the directions for the enhancement of modeling strategies.

REFERENCES

[1] K. Capellini, E. Gasparotti, U. Cella, E. Costa, B. M. Fanni, C. Groth, S. Porziani, M. E. Biancolini, S. Celi, A novel formulation for the study of the ascending aortic fluid dynamics with in vivo data, Medical Engineering and Physics (2020) S1350453320301387doi:10.1016/j.medengphy.2020.09.005.

[2] S. Zhao, W. Wu, S. Samant, B. Khan, G. S. Kassab, Y. Watanabe, Y. Murasato, M. Sharzehee, J. Makadia, D. Zolty, A. Panagopoulos, F. Burzotta, F. Migliavacca, T. W. Johnson, T. Lefevre, J. F. Lassen, E. S. Brilakis, D. L. Bhatt, G. Dangas, C. Chiastra, G. Stankovic, Y. Louvard, Y. S. Chatzizisis, Patient-specific computational simulation of coronary artery bifurcation stenting, Scientific Reports 11 (1) (2021) 16486. doi:10.1038/s41598-021-95026-2.

[3] R. Miller, E. Kerfoot, C. Mauger, T. F. Ismail, A. A. Young, D. A. Nordsletten, An implementation of patient-specific biventricular mechanics simulations with a deep learning and computational pipeline, Frontiers in Physiology 12 (2021) 716597. doi:10.3389/fphys.2021.716597.

[4] M. Loureiro-Ga, C. Veiga, G. Fdez-Manin, V. A. Jimenez, P. Juan-Salvadores, L. Busto, J. A. Baz, A. Iñiguez, Predicting tavi paravalvular regurgitation outcomes based on numerical simulation of the aortic annulus eccentricity and perivalvular areas, Computer Methods in Biomechanics and Biomedical Engineering 24 (14) (2021) 1629–1637. doi:10.1080/10255842.2021.1906233.

[5] A. Zaccaria, F. Danielli, E. Gasparotti, B. M. Fanni, S. Celi, G. Pennati, L. Petrini, Left atrial appendage occlusion device: Development and validation of a finite element model, Medical Engineering & Physics 82 (2020) 104–118. doi:10.1016/j.medengphy.2020.05.019.

[6] W. Huberts, S. G. H. Heinen, N. Zonnebeld, D. A. F. van den Heuvel, J. P. M. de Vries, J. H. M. Tordoir, D. R. Hose, T. Delhaas, F. N. van de Vosse, What is needed to make cardiovascular models suitable for clinical decision support? a viewpoint paper, Journal of Computational Science 24 (2018) 68–84. doi:10.1016/j.jocs.2017.07.006.

[7] R. A. Gray, P. Pathmanathan, Patient-specific cardiovascular computational modeling: Diversity of personalization and challenges, Journal of Cardiovascular Translational Research 11 (2) (2018) 80–88. doi:10.1007/s12265-018-9792-2.

[8] B. Spronck, J. D. Humphrey, Arterial stiffness: Different metrics, different meanings, Journal of Biomechanical Engineering 141 (9) (2019) 091004. doi:10.1115/1.4043486.

[9] A. Brault, L. Dumas, D. Lucor, Uncertainty quantification of inflow boundary condition and proximal arterial stiffness-coupled effect on pulse wave propagation in a vascular network: Uq of pulse wave propagation in a vascular network, International Journal for Numerical Methods in Biomedical Engineering 33 (10) (2017) e2859. doi:10.1002/cnm.2859.

[10] B. V. Rego, D. Weiss, M. R. Bersi, J. D. Humphrey, Uncertainty quantification in subject-specific estimation of local vessel mechanical properties, International Journal for Numerical Methods in Biomedical Engineering 37 (12) (Dec 2021). doi:10.1002/cnm.3535.

[11] B. M. Fanni, A. Pizzuto, G. Santoro, S. Celi, Introduction of a novel image-based and non-invasive method for the estimation of local elastic properties of great vessels, Electronics 11 (13) (2022) 2055. doi:10.3390/electronics11132055.

[12] B. M. Fanni, E. Sauvage, S. Celi, W. Norman, E. Vignali, L. Landini, S. Schievano, V. Positano, C. Capelli, A proof of concept of a non-invasive image-based material characterization method for enhanced patient-specific computational modeling, Cardiovascular Engineering and Technology 11 (5) (2020) 532–543. doi:10.1007/s13239-020-00479-7.

[13] S. Vulliémoz, N. Stergiopulos, R. Meuli, Estimation of local aortic elastic properties with mri: Estimation of local aortic elastic properties, Magnetic Resonance in Medicine 47 (4) (2002) 649–654. doi:10.1002/mrm.10100.

[14] S. I. Rabben, N. Stergiopulos, L. R. Hellevik, O. A. Smiseth, S. Slørdahl, S. Urheim, B. Angelsen, An ultrasound-based method for determining pulse wave velocity in superficial arteries, Journal of Biomechanics 37 (10) (2004) 1615–1622. doi:10.1016/j.jbiomech.2003.12.031.

[15] B. M. Fanni, K. Capellini, M. Di Leonardo, A. Clemente, E. Cerone, S. Berti, S. Celi, Correlation between laa morphological features and computational fluid dynamics analysis for non-valvular atrial fibrillation patients, Applied Sciences 10 (4) (2020) 1448. doi:10.3390/app10041448.

[16] M. N. Antonuccio, A. Mariotti, B. M. Fanni, K. Capellini, C. Capelli, E. Sauvage, S. Celi, Effects of uncertainty of outlet boundary conditions in a patient-specific case of aortic coarctation, Annals of Biomedical Engineering 49 (12) (2021) 3494–3507. doi:10.1007/s10439-021-02841-9.